2024 European Control Conference (ECC)
June 25-28, 2024. Stockholm, Sweden

Multi-objective optimization of individual pitch control for blade fatigue load reductions for a 15 MW wind turbine

Manuel Lara[1*], Francisco Vázquez[1], Jan-Willem van Wingerden[2], Sebastiaan Paul Mulders[2], and Juan Garrido[1]

Abstract—**In order to mitigate periodic blade loads in wind turbines, recent research has analyzed different Individual Pitch Control (IPC) approaches, which typically use the multi-blade coordinate (MBC) transformation. Some of these studies show that the introduction of an additional tuning parameter in the MBC, namely the azimuth offset, helps to decouple the nonrotating axes in the MBC transformation and enhances the IPC performance. However, these improvements have been studied without considering the increased control effort performed by the pitch signal, which is the main negative side effect of the IPC. This work addresses this trade-off between pitch signal effort and blade fatigue reduction for IPC applied to a wind turbine operating in the full load region. Here, two IPC schemes, with and without additional azimuth offset, are designed and applied to a 15 MW monopile offshore wind turbine simulated with OpenFAST software. The optimal tuning of the IPC parameters is performed by means of a multi-objective optimization solved by genetic algorithms. The optimization procedure minimizes two objective functions related to pitch signal effort and blade fatigue load. The resulting Pareto fronts show a range of optimal solutions for each IPC scheme. The selected optimal solution for IPC with azimuth offset compared to the optimal solution for IPC without offset achieves improvements of more than 10% in blade load reduction maintaining similar pitch signal effort.**

I. INTRODUCTION

Mitigating the risks associated with climate change remains a main objective for the European Union. The Union is diligently engaged in extensive efforts to markedly curtail its greenhouse gas emissions, concurrently promoting similar initiatives among other states and regions. The utilization of renewable energy sources, including solar energy, water and wind, is gaining prominence owing to their reduced environmental footprint. Electricity production contributes to approximately one-third of greenhouse gas emissions, driving the adoption of wind energy as it offers a minor ecological repercussion on the environment [1].

The detrimental impacts of structural loads, especially those induced by gravitational and aerodynamic forces, escalate with the enlargement of wind turbines and their power output. Inadequately managing structural loads may result in diminished performance or premature failure of the integral wind turbine system. Hence, it is imperative to comprehend the interplay of structural stresses, their influence on wind turbine power output, and their effects on the lifespan of the turbine. From a control viewpoint, wind turbine lifetime can be increased by reducing the different wind turbine structural loads [2].

Presently, the prevailing configuration for wind turbines consists of horizontal axis turbines equipped with three blades, operating at variable speed and variable blade pitch (VS-VP), constituting the most widespread setup [3]. Depending on the wind speed, VS-VP wind turbines transition between different operational modes or regions. In this study, particular attention is given to the full load region, highlighting the importance of minimizing the negative repercussions of increased wind speeds to protect the system from potential damage. In this scenario, it is essential to ensure that the generator speed and generator power remain at their nominal values [4].

The prevalent control strategy aimed at mitigating blade fatigue loads in wind turbines is individual pitch control (IPC) [5]. In the full load region, wind turbine speed control traditionally employs collective pitch control (CPC), where a consistent pitch value is maintained for all blades. This strategy is implemented to maintain power output at its nominal value and reject wind speed disturbances. Nevertheless, current wind turbines frequently integrate control systems that facilitate IPC for each blade [6]. An important benefit of IPC is its capability to decrease fatigue loads experienced by the tower structure, hub, and rotor blades, all while exerting minimal impact on power generation. Sensors mounted on individual blades facilitate the measurement of bending moments; nevertheless, the accuracy of these measurements is influenced by the rotating coordinate system specific to each blade. The azimuth-dependent multi-blade coordinate (MBC) transformation is commonly utilized in the majority of studies on IPC to convert the rotating moments of blades into a fixed reference frame [7]. In this non-rotating frame, two moment components are identified as the tilt moment M_t and the yaw moment M_y. IPC is implemented to decrease these two components, which are anticipated to be decoupled. Nevertheless, in real-world situations, the transformed system still exhibits coupling between these components. Some researchers incorporate an azimuth offset as an additional tuning parameter to enhance the decoupling of the multivariable system in the fixed frame [7].

An increasingly popular approach for addressing wind turbine control challenges is the utilization of computational intelligence methods [8]. In [9], a genetic algorithm (GA) optimization is implemented to adjust wind turbine controllers with the aim of minimizing the tower fore-aft displacements and the error in generator angular speed. In reference [10], the researchers applied Bayesian optimization

[1] are members of the Department of Electrical Engineering and Automation, University of Cordoba, Campus of Rabanales, 14071 Cordoba, Spain (1*corresponding author e-mail: p12laorm@uco.es)

[2] are members of Delft Center for Systems and Control, Faculty of Mechanical Engineering, Delft University of Technology, Mekelweg 2, 2628 CD Delft, The Netherlands

to optimize the controller gains and azimuth offsets within an IPC scheme, aiming to minimize the fatigue loads on the blades. In [11], a comprehensive comparison is conducted between IPC schemes, both with and without azimuth offset, ensuring equity and impartiality in the evaluation process. For this, the tuning of both IPC schemes was optimized through GAs with the sole objective of minimizing the blade fatigue load. In this comparison of both IPC schemes optimized, the simulation results demonstrated that the IPC scheme incorporating azimuth offset shows superior blade load reduction compared to the scheme without offset. These previous works study the benefits of IPC control with and without azimuth offset but they do not consider the control effort realized by the pitch signal. The main negative side effect of IPC is a higher pitch activity. A study on the trade-off between pitch signal effort and fatigue blade reduction should be addressed, which is the focus of this work.

In this study, two different IPC schemes are used to alleviate the 1P blade loads of the International Energy Agency (IEA) 15 MW Reference Wind Turbine (RWT) during operation in the full load region. In particular, the IPC parameters are tuned with the goal of simultaneously decreasing blade fatigue loading and minimizing pitch signal effort. The tuning procedure is performed by means of a multi-objective optimization (MOO) through Pareto fronts calculated with GAs. Both IPC schemes, one with azimuth offset ψ_o and the other lacking it, are subjected to optimization, analysis, and comparison. The results from both setups are evaluated against those achieved using a classical baseline PI controller, which consists in a CPC controller without IPC additions.

The paper is organized as follows: Section 2 offers background information on IPC implementation to contextualize the present work. In Section 3, the proposed methodology and the parameter tuning procedure are described. Comparative analysis of outcomes between the proposed controllers and the baseline controller is elaborated upon in Section 4, demonstrating the benefits obtained through the utilization of azimuth offset. Section 5 offers a concise summary of the conclusions drawn from the study.

II. BACKGROUND

A. MBC transformation and IPC

This section provides a concise overview of the overall design IPC and MBC transformation formulations specifically intended for mitigating 1P harmonic blade loading in three-bladed wind turbine systems. Wind turbine blade aerodynamic loads can be categorized into two distinct elements: in-plane and out-of-plane. These loads primarily emerge at multiples of (*n*-P) harmonics associated with the rotational speed of the turbine.

As depicted in Fig. 1a [12], the in-plane component aligns tangentially with the plane of rotation, whereas the out-of-plane (OoP) component extends perpendicular to it. Initially, these moments are measured within the respective rotating coordinate system of each blade, as illustrated in Fig. 1b [13], where the blade OoP bending moment at the root of the blade is referred to as My_i (with '*i*' representing the blade number, 1, 2, or 3).

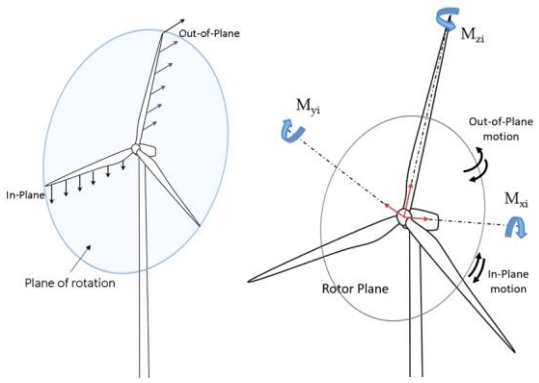

Figure 1. (a) Wind turbine blades aerodynamic loads: in-plane and out-of-plane. (b) In-plane bending moment (M_{xi}) and out-of-plane moment (M_{yi}) of the *i*-th blade.

Within the MBC transformation, the rotating OoP bending moments of the blades are compiled into the vector $\mathbf{M}(t)=[M_1(t)\ M_2(t)\ M_3(t)]^T$ and input into to the forward MBC transformation matrix $\mathbf{T}(\boldsymbol{\psi})$, as according to (1). Consequently, this procedure produces the respective azimuth-independent tilt moment (M_t (t)) and yaw moment (M_y (t)) within the fixed frame

$$\begin{bmatrix} M_t(t) \\ M_y(t) \end{bmatrix} = \boldsymbol{T}(\boldsymbol{\psi})\, \boldsymbol{M}(t). \tag{1}$$

The vector $\boldsymbol{\Psi}$ represents an array containing three azimuthal angles, with each angle corresponding to one of the three blades. A zero angle value denotes the vertical upright position. The forward transformation matrix expression is outlined in

$$\boldsymbol{T} = \frac{2}{3}\begin{bmatrix} \cos(\psi_1) & \cos(\psi_2) & \cos(\psi_3) \\ \sin(\psi_1) & \sin(\psi_2) & \sin(\psi_3) \end{bmatrix} \tag{2}$$

Subsequently, the computation of fixed frame pitch angles is performed by the IPC block, which provides the tilt- and yaw-components $\beta_t(t)$ and $\beta_y(t)$, respectively. The transformation of these two non-rotating pitch signals into the rotational frame yields the three pitch components

$$\begin{bmatrix} \beta_{IPC1}(t) \\ \beta_{IPC2}(t) \\ \beta_{IPC3}(t) \end{bmatrix} = \boldsymbol{T}^{-1}(\boldsymbol{\psi} + \psi_o)\begin{bmatrix} \beta_t(t) \\ \beta_y(t) \end{bmatrix}. \tag{3}$$

The computation of this transformation is achieved through the reverse MBC transformation in (4)..

$$\boldsymbol{T}^{-1}(\boldsymbol{\psi} + \psi_o) = \begin{bmatrix} \cos(\psi_1 + \psi_o) & \sin(\psi_1 + \psi_o) \\ \cos(\psi_2 + \psi_o) & \sin(\psi_2 + \psi_o) \\ \cos(\psi_3 + \psi_o) & \sin(\psi_3 + \psi_o) \end{bmatrix}. \tag{4}$$

The parameter ψ_o is the azimuth offset. This offset has the potential to increase the isolation of the tilt- and yaw-axis components within the fixed frame, thereby enhancing decoupling.

B. Environment for wind turbine modeling and simulation

This study involves co-simulation of a wind turbine model using MATLAB/Simulink software, with support from the OpenFAST software [14]. Specifically, we use the IEA 15 MW RWT model [15]. The key specifications of this wind turbine are as follows: it has a power rating of 15 MW, a

rated rotor speed of 7.56 rpm, and a rated wind speed of 10.59 m/s. Additionally, the pitch actuator is subject to slew-rate limits of 2 degrees per second [16]. The turbine exclusively operates in the full load region, where the blades endure significant stress, as variations in blade bending moments escalate with the mean wind speed [17], [18]. Within this specific region, the blade pitch Proportional-Integral (PI) controller adjusts the pitch to regulate the rotor speed at its rated value, while the torque controller saturates at rated torque. TurbSim is utilized to generate the turbulent wind field required for simulations [19]. Configured with a mean wind speed fixed at 18 m/s, the wind signal adopts a Kaimal turbulence spectrum with a hub turbulence intensity standing at 10%. Furthermore, it incorporates a power-law vertical shear characterized by an exponent of 0.2, with the sampling frequency adjusted to 200 Hz.

III. Proposed Methodology

The control scheme approach used in this research, depicted in Figure 2, involves the integration of two controllers: a CPC and an IPC. Through their coordinated efforts, these controllers produce the total pitch signals necessary for the efficient operation of the pitch actuators. Considering that the wind turbine operates at rated power within the full load region, the generator torque T_g remains constant at its rated value. The function of CPC is to efficiently counteract variations in wind speed and ensure that the rotor speed remains at its nominal value. A pre-designed gain-scheduling PI controller derived from the Reference OpenSource Controller (ROSCO) is adopted for the CPC in this study [20]. The IPC block effectively diminishes the cyclic blade loads associated with various harmonics. Illustrated in Figure 3, the IPC scheme implemented in this research integrates MBC transformations specifically designed to mitigate the 1P harmonic, a decentralized control, and the reverse MBC transformation incorporating azimuth offset.

The MBC transformation calculates M_t and M_y moments within a fixed frame using the measured OoP blade moments in the rotating frame. The decentralized control consists of two pure integral controllers to mitigate the M_t and M_y moments while simultaneously generating the corresponding β_t and β_y pitch signals. A different gain is used in each integral controller. Therefore, the suggested 1P IPC scheme involves the tuning of two integral gains: k_{I_tilt} and k_{I_yaw}. These variables serve as decision variables in the optimization process when there is no azimuth offset. Subsequently, the calculated non-rotating tilt and yaw pitch signals for each harmonic are processed using the reverse MBC transformation, producing three distinct blade pitch angles suitable for implementation within the rotating frames. The utilization of azimuth offset in the reverse MBC transformation introduces an extra parameter for optimization in the 1P IPC scheme: the azimuth offset (ψ_o).

Employing azimuth offset aims to enhance the decoupling of the tilt and yaw axes, potentially resulting in a more significant reduction in periodic blade loads compared to the IPC scheme without offset (ψ_o= 0º). Finally, the IPC signals are combined with the CPC value to compute the total pitch angle for the individual blades.

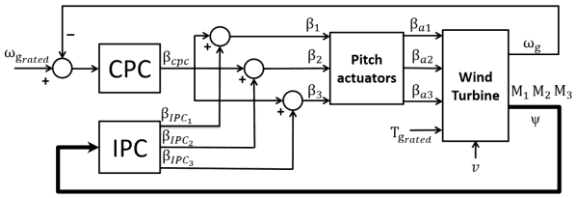

Figure 2. IPC+CPC control system scheme for the full load region.

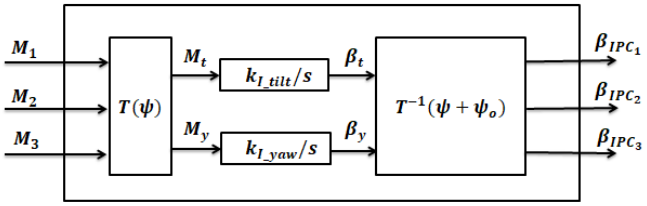

Figure 3. 1P IPC scheme with azimuth offset.

A. IPC tuning procedure by multi-objective optimization

In this section, the multi-objective optimization framework for finding the optimal set of IPC controller parameters is described. The main benefit of IPC is the reduction of blade load fatigue, however, at the expense of increased pitch activity and actuator stresses. In this paper, the trade-off between fatigue blade reduction and pitch signal effort in IPC is addressed as a MOO problem. The approach to this optimization problem involves the introduction of two objective functions to minimize within the cost function vector $\boldsymbol{J}$= *[DEL(M_{y1}) TV(β_1)]*.

The first objective function, DEL(M_{y1}), aims to minimize blade fatigue loading by focusing on the fatigue damage equivalent load (DEL) and concentrating on the OoP moment of the blades along the y-axis, as depicted in Fig. 1b. For fatigue assessment of wind turbines, the DEL index is usually calculated offline from time series of simulation data using cycle counting techniques, and therefore, it cannot be evaluated analytically. The MLife suite of scripts [21] is utilized for the post-processing of data from each simulation, facilitating the extraction of the corresponding DEL values.

The duty cycle of the pitch signal experiences a significant boost with the IPC schemes in comparison to the CPC. This elevated level of activity can be quantified through the calculation of the total variation (TV) of the pitch according to

$$TV(\beta_1) = \frac{1}{t_{sim}-t_0}\int_{t_0}^{t_{sim}} \left|\frac{d\beta_1(t)}{dt}\right| dt, \qquad (5)$$

which is the second objective in the cost function vector **J**. Its purpose is to discourage control designs that cause considerable oscillations in the total pitch signal.

Two variations of the IPC are calibrated for later comparison: one without azimuth offset and the other with azimuth offset ψ_o. The first one, has the two-parameter vector $\boldsymbol{\rho}$ = [k_{I_tilt}, k_{I_yaw}] with the integral gains; the second one, IPC with azimuth offset, also has the offset ψ_o as additional parameter in the decision variable vector $\boldsymbol{\rho}$ = [k_{I_tilt}, k_{I_yaw}, ψ_o] to be optimized.

The resolution of this MOO problem adheres to the methodology delineated in Fig. 4. It involves computing

Pareto fronts and employing decision makers to discern the ultimate satisfactory solution. Owing to the complexity of the proposed objective functions in J, as well as the intricate nature of the wind turbine dynamic model, analytical evaluation is infeasible. Consequently, the calculation of Pareto front solutions is conducted through a simulation-based approach utilizing an optimizer. This approach requires conducting numerous co-simulations with OpenFAST and Simulink.

The first step involves initializing the decision variables in vector $\boldsymbol{\rho_0}$. Subsequently, the procedure moves into an iterative loop for optimization, during which the MATLAB optimizer carries out diverse simulations employing FAST/Simulink to compute the cost function **J** and explore solutions across the Pareto front. The optimization procedure evolves into a nonlinear problem demanding substantial computational resources and time. The optimization procedure adopts the nondominated sorting genetic algorithm-II (NSGA-II) to improve computational efficiency. NSGA-II is an evolutionary algorithm designed specifically for MOO [22]. NSGA-II efficiently explores the multi-objective solution space, categorizes solutions into non-dominated fronts, and balances exploration and exploitation to find a varied array of high-quality solutions for multi-objective optimization problems. NSGA-II manages to maintain diversity in the population by using selection, crossover, and mutation operators. Selection ensures diversity among the solutions. Crossover and mutation operations create new offspring solutions, which are added to the population and replace less fit solutions, driving the evolution process.

Pareto frontier solutions are subject to assessment and prioritization through the utilization of multi-criteria decision-making (MCDM) methodologies, facilitating the selection of the most preferable option according to individual preferences. Among these methods, the Technique for Order of Preference by Similarity to Ideal Solution (TOPSIS) is frequently employed within the energy sector in numerous research. The result obtained with the TOPSIS method is chosen as the optimal solution $\boldsymbol{\rho}^*$.

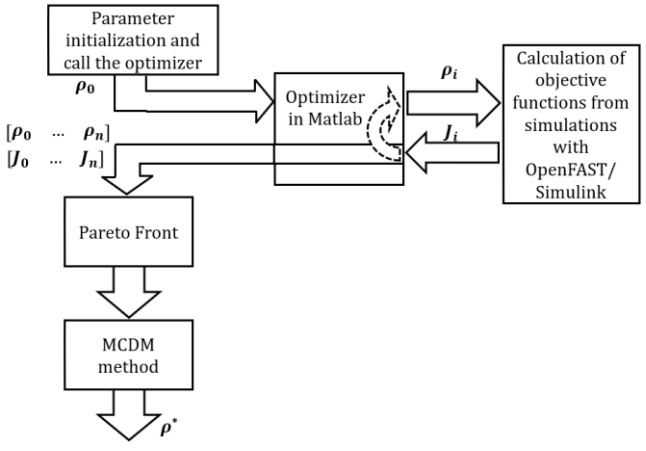

Figure 4. Multi-objective optimization procedure.

In the exploration process, the integral gains are examined within the interval of [0-0.005] $\text{rad}\cdot\text{Nm}^{-1}\text{s}^{-1}$ and simultaneously, the azimuth offset is examined across the span of [0º-90º]. The key parameters defined in the GA configuration include a population size consisting of 200 individuals, a maximum generation limit set to 50, a crossover fraction of 0.75 and a Pareto front population fraction of 12.5%.

IV. Results

A. Multi-objective optimization results

This section shows the multi-objective optimization results of the proposed IPC schemes. Figure 5 shows the Pareto fronts obtained for the two IPC schemes under study: without azimuth offset and with it. In each front, the chosen best solution is highlighted with a star. To choose the optimal solutions for each IPC scheme we proceed as follows: the optimal solution from the Pareto front of IPC without ψ_o is chosen through the TOPSIS method (blue star). Then, the optimal solution from the Pareto front of IPC with ψ_o (red star) is proposed as the solution that has a similar TV(β_1) as that of the optimal IPC without ψ_o. Ideally, this would be equivalent to calculate the intersection of this Pareto front (red points) with a horizontal line from the optimal solution (blue star) of the IPC without azimuth. Table I exhibits the optimal control parameters for both versions of IPC. Incorporating azimuth offset in the IPC enhances the indices, as the attained Pareto front solutions exhibit lower index values compared to those achieved using IPC without offset. Pareto front of IPC with offset displays a more pronounced leftward displacement, indicating the achievement of lower TV(β_1) values with no change in the DEL(M_{y1}) value.

Figure 6 shows the control parameters obtained for each point of the Pareto fronts of Fig. 5 represented regarding the objective function DEL(M_{y1}). The first two plots show the integral gains k_{I_tilt} and k_{I_yaw} for both IPC schemes, and the third plot shows the azimuth offset ψ_o for the IPC with offset. For both IPC schemes, the plots indicate that within a specific allowed range, the higher the integral gains, the lower the DEL(M_{y1}). Including azimuth offset allows for a wider range of k_{I_tilt}, enabling lower DEL(M_{y1}) values.

TABLE I. Optimal IPC parameters.

IPC scheme	k_{I_tilt} ($\text{rad}\cdot\text{kNm}^{-1}\text{s}^{-1}$)	k_{I_yaw} ($\text{rad}\cdot\text{kNm}^{-1}\text{s}^{-1}$)	ψ_o (deg)
IPC (no ψ_o)	$2.35\cdot10^{-7}$	$1.65\cdot10^{-8}$	0
IPC with ψ_o	$1.39\cdot10^{-6}$	$1.84\cdot10^{-8}$	49.03

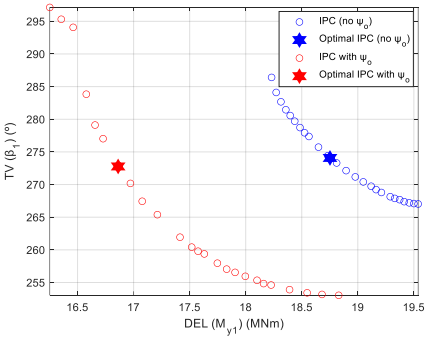

Figure 5. Pareto fronts for CPC+IPC with ψ_o (red points) and CPC+IPC without ψ_o (blue points)

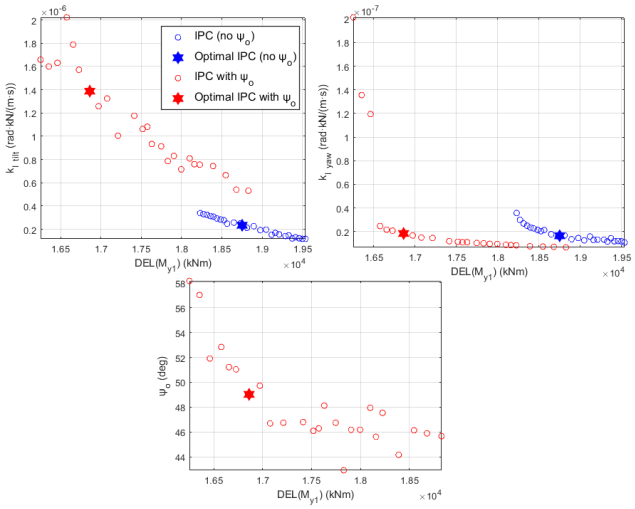

Figure 6. Control parameters obtained for IPC with ψ_o (red points) and IPC without ψ_o (blue points)

B. *Simulation results*

This section analyses the simulation outcomes of the optimized IPC schemes that have been adjusted using the previous optimal parameters shown in Table I. Table II presents the TV(β_1) and DEL (M_{y1}) resulting from the optimal solutions for a simulation of 600 s. Table II shows the DEL (M_{y1}) and TV(β_1) obtained from the optimal solutions for a simulation of 600 s. Other indices are also calculated such as the standard deviations (STD) of the generated power (P_g), the STD of M_{y1}, and the total variation of M_{y1}. Additionally, Table II also shows their percentage values with respect to the baseline case (CPC without IPC). The IPC without azimuth offset achieves a 25.5% reduction in DEL(M_{y1}) with respect to the baseline case. The IPC with azimuth offset outperforms the previous one and achieves a 33.07% reduction in DEL(M_{y1}). This is a 10.08% reduction with respect to the case of IPC without ψ_o while maintaining a similar pitch total variation.

Figure 7 shows the simulated time responses of the analyzed control strategies. For clarity, only 100 s of the entire 600 s of the simulation are represented. The plots show the wind speed ν, the generated power P_g, the generator speed ω_g, the blade OoP bending moments of blade 1 M_{y1}, and the pitch signal of blade 1 β_1. The moments M_{y1} are reduced with both IPC strategies. The DEL(M_{y1}) index is reduced more than 25% maintaining similar standard deviations of generated power. However, this result is achieved at the expense of a higher pitch activity with higher values of TV(β_1). The IPC with azimuth offset obtains the best performance for DEL(M_{y1}), STD(M_{y1}) and TV(M_{y1}). Figure 7 also shows that there is substantial overlap between the responses of the generated power and speed, indicating that the IPC strategies do not disrupt the operation of the CPC.

The Fourier spectra of the blade OoP bending moment and the pitch signal of blade 1 are illustrated in Figure 8. The comparison with the CPC reveals that both IPC schemes effectively suppress the significant 1P-component peak of the blade moment near the frequency of 0.126 Hz, as depicted in Fig. 9(a). Regarding the pitch signal, the CPC does not exhibit peak values at the 1P frequency. Both IPC schemes exhibit a notable peak value attributed to the 1P-component of the pitch, which primarily contributes to the prominent pitch activity.

TABLE II. COST FUNCTIONS AND OTHERS PERFORMANCE INDEXES.

Control	Baseline CPC	IPC (no ψ_o)	IPC with ψ_o
DEL(M_{y1}) (kNm)	$2.51 \cdot 10^4$	$1.87 \cdot 10^4$ (74.5% CPC)	$1.68 \cdot 10^4$ (66.9% CPC) (89.8% IPC no ψ_o)
TV(β_1) (deg)	38.47	274.07 (712.2% CPC)	272.77 (709.0% CPC)
STD(P_g) (kW)	608.70	609.23 (100.1% CPC)	610.25 (100.3% CPC)
STD(M_{y1}) (kNm)	$7.41 \cdot 10^3$	$5.47 \cdot 10^3$ (73.8% CPC)	$5.06 \cdot 10^3$ (68.3% CPC)
TV(M_{y1}) (kNm)	$3.45 \cdot 10^6$	$3.27 \cdot 10^6$ (94.8% CPC)	$3.23 \cdot 10^6$ (93.6% CPC)
Range(M_{y1}) (kNm)	$4.57 \cdot 10^4$	$3.19 \cdot 10^4$ (69.8% CPC)	$2.94 \cdot 10^4$ (64.3% CPC)

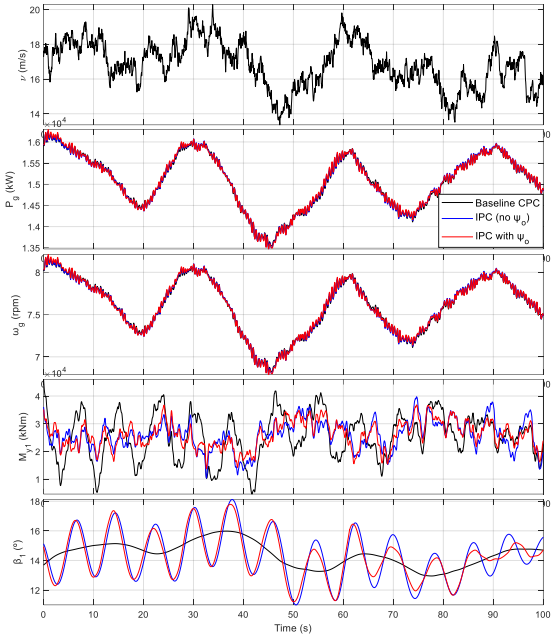

Figure 7. Time responses of the wind speed, generated power, generator speed, out-of-plane bending moment of blade 1, and pitch signal of blade 1.

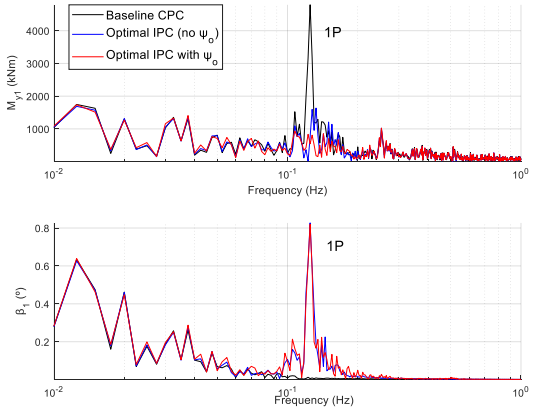

Figure 8. Comparison of the Fourier spectra of the OoP blade moment and the pitch signal for blade 1.

V. CONCLUSION

This work deals with the main problem of IPC for blade load reduction: the trade-off between the blade load fatigue and the pitch signal effort. The parameter tuning procedure of two 1P IPC schemes, with and without azimuth offset, is formulated as a multi-objective optimization. Genetic algorithms are employed to solve the problem, aiming to attain Pareto front solutions while considering two objective functions: the DEL index of the out-of-plane bending moment, which is related to the blade fatigue load; and the total variation of the pitch signal, which is related to the fluctuations of the pitch actuator effort. The IPC schemes are combined with a pre-defined CPC, which is not modified, to regulate the generator speed at its rated value. Both controllers integrate a complete block IPC+CPC.

Among the Pareto front solutions of the IPC without azimuth offset, the TOPSIS method is used as MCDM tool to determine the optimal compromise solution that satisfactorily addresses both of these objectives. This solution is considered the optimal solution for IPC without azimuth offset. From the Pareto front solutions of the IPC with azimuth offset, the optimal solution is chosen as the solution that maintains a similar value of pitch signal effort as the optimal solution for IPC without azimuth offset.

Analysis of the simulation results for the optimal IPC solutions involves both qualitative and quantitative comparison. This comparison reveals that IPC does not impact the ability of the CPC to regulate the generated power, while significantly enhancing the decrease of out-of-plane blade moments, although this comes with the consequence of increased pitch signal activity. Comparing both optimal IPC solutions reveals that the IPC without azimuth offset produces inferior results relative to the IPC with offset. The IPC with offset can achieve a significant decrease in 1P component moments while maintaining a comparable level of control effort of the pitch signal. Therefore, it can be concluded that the incorporation of optimal azimuth offset in the IPC scheme surpasses the response of the IPC scheme even when this is also optimized. In this study, the resulting improvements are around 10% in the DEL index of out-of-plane blade moments, with similar total variation of the pitch signal.

ACKNOWLEDGMENT

This work was supported by the Spanish Ministry of Science and Innovation under Grant PID2020-117063RB-I00/AEI/10.13039/501100011033.

REFERENCES

[1] M. Lara, F. Vázquez, I. Sandua-Fernández, and J. Garrido, "Adaptive Active Generator Torque Controller Design Using Multi-Objective Optimization for Tower Lateral Load Reduction in Monopile Offshore Wind Turbines," IEEE Access, vol. 11, pp. 115894–115910, 2023, doi: 10.1109/ACCESS.2023.3325840.

[2] J. G. Njiri and D. Söffker, "State-of-the-art in wind turbine control: Trends and challenges," Renew. Sustain. Energy Rev., vol. 60, pp. 377–393, Jul. 2016, doi: 10.1016/j.rser.2016.01.110.

[3] A. Gambier, "Pitch Control of Three Bladed Large Wind Energy Converters—A Review," Energies, vol. 14, no. 23, p. 8083, Dec. 2021, doi: 10.3390/en14238083.

[4] E. J. Novaes Menezes, A. M. Araújo, and N. S. Bouchonneau da Silva, "A review on wind turbine control and its associated methods," J. Clean. Prod., vol. 174, pp. 945–953, Feb. 2018, doi: 10.1016/j.jclepro.2017.10.297.

[5] E. A. Bossanyi, "Wind Turbine Control for Load Reduction," Wind Energy, vol. 6, no. 3, pp. 229–244, Jul. 2003, doi: 10.1002/we.95.

[6] O. Apata and D. T. O. Oyedokun, "An overview of control techniques for wind turbine systems," Sci. African, vol. 10, p. e00566, Nov. 2020, doi: 10.1016/J.SCIAF.2020.E00566.

[7] S. P. Mulders, A. K. Pamososuryo, G. E. Disario, and J.-W. van Wingerden, "Analysis and optimal individual pitch control decoupling by inclusion of an azimuth offset in the multiblade coordinate transformation," Wind Energy, vol. 22, no. 3, pp. 341–359, Mar. 2019, doi: 10.1002/we.2289.

[8] C. Serrano, J.-E. Sierra-Garcia, and M. Santos, "Hybrid Optimized Fuzzy Pitch Controller of a Floating Wind Turbine with Fatigue Analysis," J. Mar. Sci. Eng., vol. 10, no. 11, p. 1769, Nov. 2022, doi: 10.3390/jmse10111769.

[9] M. Lara, J. Garrido, M. L. Ruz, and F. Vázquez, "Adaptive Pitch Controller of a Large-Scale Wind Turbine Using Multi-Objective Optimization," Appl. Sci., vol. 11, no. 6, p. 2844, Mar. 2021, doi: 10.3390/app11062844.

[10] S. Mulders, A. Pamososuryo, and J. van Wingerden, "Efficient tuning of Individual Pitch Control: A Bayesian Optimization Machine Learning approach," J. Phys. Conf. Ser., vol. 1618, no. 2, p. 022039, Sep. 2020, doi: 10.1088/1742-6596/1618/2/022039.

[11] M. Lara, S. P. Mulders, J.-W. van Wingerden, F. Vázquez, and J. Garrido, "Analysis of Adaptive Individual Pitch Control Schemes for Blade Fatigue Load Reduction on a 15 MW Wind Turbine," Appl. Sci., vol. 14, no. 1, p. 183, Dec. 2023, doi: 10.3390/app14010183.

[12] J. Jeong, K. Park, S. Jun, K. Song, and D.-H. Lee, "Design optimization of a wind turbine blade to reduce the fluctuating unsteady aerodynamic load in turbulent wind," J. Mech. Sci. Technol., vol. 26, no. 3, pp. 827–838, Mar. 2012, doi: 10.1007/s12206-011-1106-4.

[13] J. Cheon, J. Kim, J. Lee, K. Lee, and Y. Choi, "Development of Hardware-in-the-Loop-Simulation Testbed for Pitch Control System Performance Test," Energies, vol. 12, no. 10, p. 2031, May 2019, doi: 10.3390/en12102031.

[14] "OpenFAST," OpenFAST v3.2.0 documentation. https://openfast.readthedocs.io/en/main/ (accessed Oct. 26, 2022).

[15] R. Niranjan and S. B. Ramisetti, "Insights from detailed numerical investigation of 15 MW offshore semi-submersible wind turbine using aero-hydro-servo-elastic code," Ocean Eng., vol. 251, p. 111024, May 2022, doi: 10.1016/j.oceaneng.2022.111024.

[16] F. Papi and A. Bianchini, "Technical challenges in floating offshore wind turbine upscaling: A critical analysis based on the NREL 5 MW and IEA 15 MW Reference Turbines," Renew. Sustain. Energy Rev., vol. 162, p. 112489, Jul. 2022, doi: 10.1016/j.rser.2022.112489.

[17] L. Bergami and M. Gaunaa, "Analysis of aeroelastic loads and their contributions to fatigue damage," J. Phys. Conf. Ser., vol. 555, p. 012007, Dec. 2014, doi: 10.1088/1742-6596/555/1/012007.

[18] A. Natarajan, "Damage equivalent load synthesis and stochastic extrapolation for fatigue life validation," Wind Energy Sci., vol. 7, no. 3, pp. 1171–1181, Jun. 2022, doi: 10.5194/wes-7-1171-2022.

[19] B. J. Jonkman, "Turbsim User's Guide: Version 1.50," Sep. 2009, doi: 10.2172/965520.

[20] NREL, "NREL's Reference OpenSource Controller (ROSCO) toolbox for wind turbine applications.," 2019.

[21] J. G. Hayman, and J. M. Buhl, "Mlife users guide for version 1.00," National Renewable Energy Laboratory, Golden, CO, 2012, vol. 74, no 75, p. 112. https://www.nrel.gov/wind/nwtc/mlife.html (accessed Apr. 25, 2023).

[22] K. Deb, A. Pratap, S. Agarwal, and T. Meyarivan, "A fast and elitist multiobjective genetic algorithm: NSGA-II," IEEE Trans. Evol. Comput., vol. 6, no. 2, pp. 182–197, Apr. 2002, doi: 10.1109/4235.996017.